

HOMOLOGY MODELING AND MOLECULAR  
MECHANICS OF THE  $bc_7$  COMPLEX

By

BYRON N. QUINN

Bachelor of Science

Langston University

Langston, Oklahoma

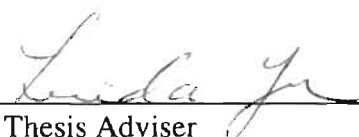
1997

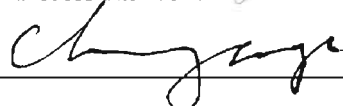
Submitted to the Faculty of the  
Graduate College of the  
Oklahoma State University  
in partial fulfillment of  
the requirements for  
the Degree of  
MASTER OF SCIENCE  
December, 2000

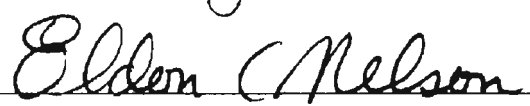
---

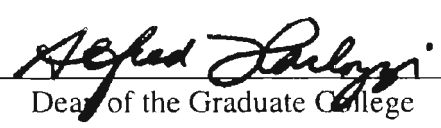
HOMOLOGY MODELING AND MOLECULAR  
MECHANICS OF THE  $bc_1$  COMPLEX

Thesis Approved:

  
Thesis Adviser





  
Dean of the Graduate College

## ACKNOWLEDGMENTS

I would like to thank my advisor, Dr. Linda Yu for her highly sophisticated supervision and guidance. I am also just as thankful to Dr. Chang-an Yu for his fascinating ability to encourage and motivate my pursuit of knowledge in science. My extreme appreciation goes out to my other committee member, Dr. Eldon C. Nelson an extraordinary and wonderful individual indeed, for all of his advice and guidance. I would also like to extend many thanks to my parents for their support and encouragement. To Dr. Steve White, a very brilliant individual, I would like to say thanks for all your help. I would also like to thank Dr. Di Xia for all of his support, guidance and advice.

Finally, I want to thank the National Institute of Health for providing the resources for me to conduct research and pursue this degree.

## TABLE OF CONTENTS

Chapter	Page
I. HOMOLOGY MODELING OF BACTERIAL CYTOCHROME <i>bc<sub>1</sub></i> COMPLEX.....	1
Introduction.....	1
Methodology.....	5
Results and discussion.....	6
Conclusion.....	16
References.....	17
II. MOLECULAR MECHANICS OF THE CYTOCHROME <i>bc<sub>1</sub></i> COMPLEX.....	20
Introduction.....	20
Methodology.....	23
Results and discussion.....	24
Conclusion.....	41
References.....	42

## LIST OF TABLES

Table	Page
I. Cytochrome <i>b</i> Heme Analysis .....	25
II. Potential Energy Values for ISP at Different Redox States.....	28
III. ISP Torsion Angle Analysis.....	28

## LIST OF FIGURES

Figure	Page
1. Bovine $bc_1$ complex.....	4
2. Sequence Alignment of Cytochrome $b$ . ....	7
3. Bovine Cytochrome $b$ and Core 1.....	8
4. <i>Rs.</i> Cytochrome $b$ first insertion.....	8
5. Bovine Cytochrome $b$ and subunit 6.....	8
6. <i>Rs.</i> Cytochrome $b$ fourth insertion.....	8
7. Sequence Alignment for Cytochrome $c_1$ .....	10
8. Cytochrome $c_1$ .....	10
9. Iron Sulfur Protein Sequence Alignment.....	11
10. ISP 3D structure.....	11
11. Bovine Cytochrome $b$ and Subunit 7.....	13
12. <i>R. sphaeroides</i> cytochrome $b$ and subunit 4.....	13
13. AOR .....	13
14. Sequence Alignment for AOR and <i>Rs</i> Subunit 4.....	14
15. AOR structural homology.....	14
16. Bovine core 1 structural homology.....	14
17. CSN sequence alignment of bovine core1 with <i>Rs.</i> subunit 4.....	14
18. <i>R. sphaeroides</i> subunit 4 with CSN templet.....	15
19. Theoretical model of the <i>R. sphaeroides</i> $bc_1$ Complex.....	15

Figure	Page
20. Cytochrome <i>bc</i> <sub>1</sub> complex redox groups.....	22
21. Iron Sulfur Cluster.....	22
22. Cytochrome <i>b</i> redox state comparison.....	26
23. Cytochrome <i>c</i> <sub>1</sub> redox state comparison.....	26
24. Cytochrome <i>c</i> <sub>1</sub> redox state comparison with original structure (1QCR).....	29
25. ISP with both irons reduced.....	29
26. Relative position of ISP with both iron atoms reduced.....	29
27. ISP [2-3] comparison.....	31
28. ISP [2-3] relative position.....	31
29. ISP [2-2] and [2-3] overall comparison.....	31
30. ISP [3-3] comparison.....	32
31. ISP [3-3] and [2-3].....	32
32. ISP [3-2] comparison.....	32
33. Protein back bone torsion angles.....	36
34. ISP linker regions.....	36
35. 2Fe2S cluster electron density.....	37
36. ISP density at serine 61 region.....	37
37. ISP density at serine 65 region.....	37
38. ISP neck region density .....	39
39. ISP electron density at residues 86-88 and 90-92.....	40

## NOMENCLATURE

AFR	Aldehyde Ferredoxin Oxidoreductase
Cys-Fe	Iron atom coordinated to the cysteines
CSN	Closest structural neighbor
His-Fe	Iron atom coordinated to the histidines
ISP	Iron sulfur protein
ISP [2-2]	Cys-Fe reduced and his-Fe reduced
ISP [2-3]	Cys-Fe reduced and his-Fe oxidized
ISP [3-2]	Cys-Fe oxidized and his-Fe reduced
ISP [3-3]	Cys-Fe oxidized and his-Fe oxidized
Rs.	<i>Rhodobactor sphaeroides</i>



## CHAPTER I

### HOMOLOGY MODELING OF BACTERIA *bc<sub>1</sub>* COMPLEX

#### Introduction

##### I. Homology Modeling

Homology modeling is a technique used to predict the three-dimensional structure of a protein. Structure prediction is accomplished by swapping the three-dimensional coordinates from a homologous reference protein. The underlying principle in homology modeling is that sequence conservation is directly proportional to structural conservation. Early work in homology modeling successfully took advantage of this basic fundamental principle (1,2). As homology modeling techniques developed it was found that by using more than one protein from different species for the reference protein one could locate regions of structural conservation more effectively (3-7). In order to successfully model a protein with homology modeling techniques one will need a sequence alignment with greater than 50% residue identity for better confidence in the resulting structure but 20-30% is acceptable if several aligned sequences and structures are available (8).

Homology modeling has been used in the understanding of drug resistance in malaria: three-dimensional structure of *Plasmodium falciparum* dihydrofolate reductase by homology building where the significance of the most important point mutation causing resistance could be explained by the model (9). Homology modeling has also been used in the modeling of the insect chitinase catalytic domain oligosaccharide complex that led to the identification of an active-site amino acid residue (10).

In homology modeling there may be sequence insertions in the model that is being built. To overcome the problem of not being able to assign coordinates to this region where the insertions are a technique of closest three-dimensional (3D) structural neighbor (CSN) will be used to find a possible structure for the insertions. Basically, in CSN the coordinates for the insertions are obtained from nearby subunits in the reference protein.

## II. Cytochrome $bc_1$ complex

The complex that will be modeled here by the use of homology modeling is the *Rhodobacter sphaeroides* (Rs.) ubiquinone cytochrome *c* oxidoreductase ( $bc_1$  complex). The  $bc_1$  complex is a transmembrane protein that passes electrons from ubiquinol to cytochrome *c*. Cytochrome  $bc_1$  complex couples this electron transfer to proton translocation across biological membranes to generate a proton gradient and membrane potential for ATP synthesis. This redox-linked proton pump is a critical component of eukaryotic respiratory system. The  $bc_1$  complex also plays a critical role in the photosynthetic and/or respiratory systems of various prokaryotes. Bovine cytochrome  $bc_1$  complex consists of 11 subunits with a molecular weight of close to 250 kDa. *R. sphaeroides* cytochrome  $bc_1$  complex consists of 4 subunits with a molecular weight close to 110 kDa. The bovine  $bc_1$  complex will be used as a template to model the *R. sphaeroides*  $bc_1$  complex. Three subunits that have been found to be essential for catalytic functioning of the cytochrome  $bc_1$  complex are cytochrome *b*, cytochrome  $c_1$ , and the iron sulfur protein (ISP). Cytochrome *b*, cytochrome  $c_1$ , and ISP are the three subunits with highest sequence homology between the bovine  $bc_1$  complex and the *R.*

*sphaeroides bc<sub>1</sub>* complex. *R. sphaeroides* fourth subunit, subunit 4, does not have significant homology with any of the other subunits in the bovine *bc<sub>1</sub>* complex. However, subunit 4 in the *R. sphaeroides bc<sub>1</sub>* complex has chemical and physical features similar to that of subunit 7 in the bovine *bc<sub>1</sub>* complex. Both of these subunits are known to be photo-affinity labeled by azido-quinone (11-14).

The bovine heart and chicken mitochondrial *bc<sub>1</sub>* complex structures were previously reported and will be used as a template to model the *R. sphaeroides bc<sub>1</sub>* complex (15-17). The structure of the bovine *bc<sub>1</sub>* complex is shown in (Figure 1) (15). X-ray diffraction studies from the bovine cytochrome *bc<sub>1</sub>* complex have had a profound impact on the understanding of how this complex functions. Early diffraction studies provided new insights into the head domain mobility that has recently been found to be important for catalytic functioning of the cytochrome *bc<sub>1</sub>* complex (15). Inhibitor x-ray diffraction studies have allowed a preliminary understanding of the active sites in the cytochrome *bc<sub>1</sub>* complex (18).

The ability to perform mutagenesis studies on the *R. sphaeroides bc<sub>1</sub>* complex to understand how this complex function is possible and very efficient. It is important to have a model structure of the *R. sphaeroides bc<sub>1</sub>* complex to aid in the process of locating residues to mutate based upon logical theories. The model structure will help to predetermine the possible effect of a mutation in order to determine if valuable resources should be deployed to develop mutants. A model of this complex will also prove to be extremely useful for doing computational molecular mechanics and dynamic simulations to elucidate conformational aspects of the complex that relates to function. It is less time consuming to run simulations on the bacterial *bc<sub>1</sub>* complex because of its size only four

subunits relative to the bovine *bc<sub>1</sub>* complex eleven subunits. Having the tertiary structure of a protein also allows one to be more effective in developing a complete understanding of the complex functional attributes of a protein.

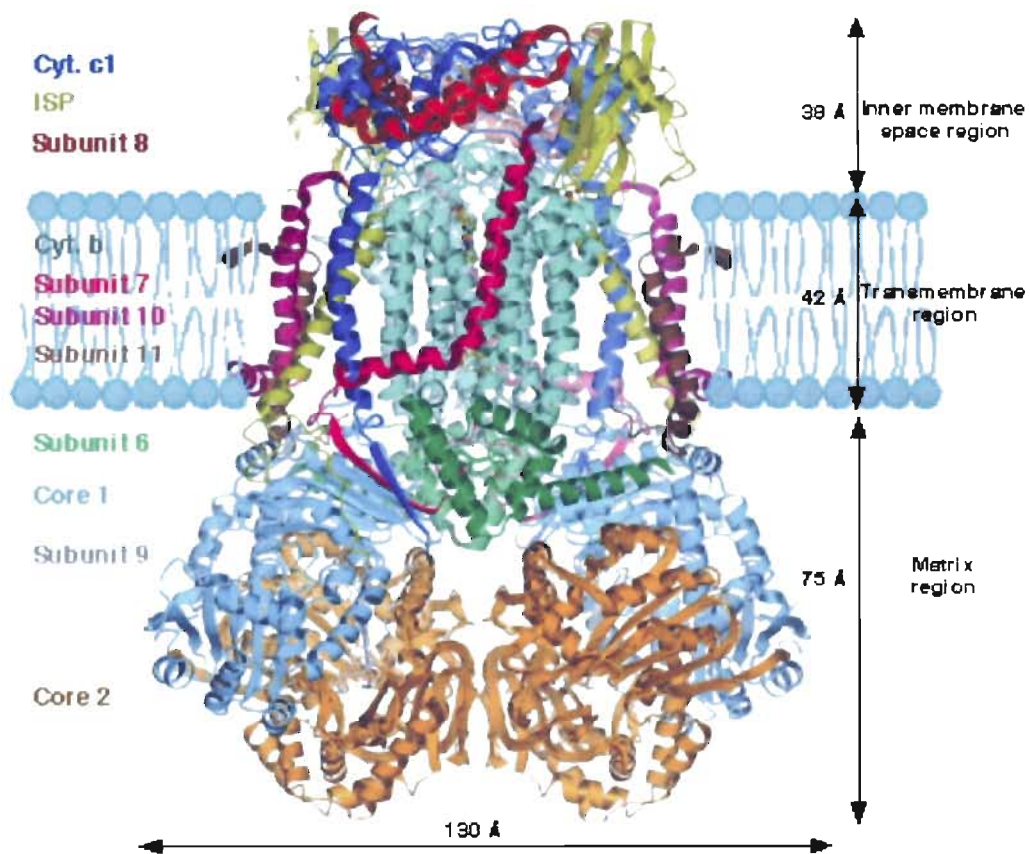


Figure 1. Bovine *bc<sub>1</sub>* complex.

## Methodology

The programs that are used to build the model are crystallographic program O and molecular modeling program InsightII. The x-ray coordinates from the refined bovine *bc<sub>1</sub>* complex 1QCR (not yet released) were used as a template. The first step is sequence alignment by Blast and modifications as necessary by visual inspection to minimize the insertions and deletions in the sequence alignment (19). The second step is to swap coordinates from the template to the model in all regions where there is a corresponding match in the sequence alignment. The third step consists of building regions of the sequence alignment where there is an insertion in the model sequence. Two methods were used to determine the structure for the area of insertions. The first is to find the CSN in the template which will usually for this project consist of an structural element from another subunit that is in the general vicinity of this insertion area. The second method is to model a loop or use secondary structure prediction software for the insertion and use molecular dynamics calculations to find a likely position for the region. In finding secondary structure for unaligned sequence InsightII homology module for secondary structure prediction is used.

## Results and Discussion

### I. Cytochrome *b*

The first subunit modeled is cytochrome *b*. *R. sphaeroides* cytochrome *b* sequence is larger than that of bovine cytochrome *b*. There are four insertions in the sequence alignment as seen in (Figure 2). The first insertion is at the beginning of the sequence, at residues 1-15 in the *R. sphaeroides* cytochrome *b*. In order to assign coordinates to this part of the sequence the CSN was located. The closest structural neighbor in the template, bovine *bc<sub>1</sub>* complex, is the C-terminal of core1 residues 429 - 443. From secondary structure prediction, *R. sphaeroides* cytochrome *b* residues 1-15 have a high propensity for a helix and there is a helix in this part of core1 (Figure 3 and 4). The second insertion in the *R. sphaeroides* cytochrome *b* is at residues 232-239 (Figure 2). The residues in the second insertion also show a high propensity for a helix. The CSN is a helix from subunit 6 residues 59-66 of bovine. The third insertion in *R. sphaeroides* cytochrome *b* is between residues 309-326 (Figure 2). These residues show some propensity for a beta sheet but there is no CSN for these residues and no other beta sheets in this area. Therefore, the third insertion is modeled in as a random loop and molecular dynamics are performed to find a favorable random position for this loop. The fourth insertion is at the C-terminal of the *R. sphaeroides bc<sub>1</sub>* complex residues 422 - 445 (Figure 2). The CSN are residues 17-40 in subunit 6 of bovine (Figure 5). Therefore, these residues coordinates were used (Figure 6).



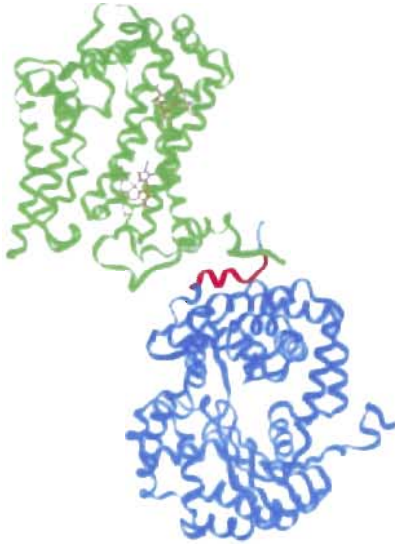


Figure 3. Bovine cytochrome *b* and core 1. In blue core 1 with the CSN of core 1 C-term colored in red. In green cytochrome *b*.



Figure 4. Rs. cytochrome *b* first insertion. The color red denotes the location of the first insertion.



Figure 5. Bovine cytochrome *b* and subunit 6. Where cytochrome *b* is green and subunit 6 is blue with CSN in red.



Figure 6. Rs. cytochrome *b* fourth insertion. In red is the CSN template from bovine subunit 6.



## II. Cytochrome $c_1$

The next subunit modeled is cytochrome  $c_1$ . Cytochrome  $c_1$  has one major insertion at residues 141 - 161 (Figure 7). The secondary structure prediction for this region shows a random coil. The CSN for this insertion is in subunit eight of bovine residues 34 – 54 (Figure 8). This particular subunit is believed to be important for the docking of cytochrome  $c$  on the  $bc_1$  complex.

## III. ISP

The third subunit modeled is ISP. The ISP subunit has 1 major insertion at residues 96 – 107 (Figure 9). These residues show a high propensity for a helix but no noticeable CSN. This helix was subsequently modeled in. The insertion in *R. sphaeroides* ISP that has no noticeable CSN is relatively close to the insertion in the *R. sphaeroides* cytochrome  $b$  subunit that also does not have a noticeable CSN. It is possible that these two insertions could interact with each other. Future modeling and site directed mutagenesis will help to determine whether these two insertions have any interactions of any importance. It is known that the ISP head domain docks on the cytochrome  $b$  subunit, thus the insertion in ISP may be important in this docking process.

<i>RHOSH_cyt c1</i> :	AGGGHVEDV	PFSFEGPFGT	FDQHQLQRGL	QVYTEVCAAC	HGMKFVPIRS	LSEPGGPELP
<i>BOVIN_cyt c1</i> :	SDLELHPPSY	PWSHRGLLSS	LDHTSIRRGF	QVYKQVCSSC	HSMDYVAYRH	LVGVCYTEDE
<i>RHOSH_cyt c1</i> :	EDQVRAYATQ	FTVTDEETGE	D-REGKPTDH	FPHSALENAA	DLSLMAKARA	GFHGPMGTGI
<i>BOVIN_cyt c1</i> :	AKALAEVEEV	QDGPNEDEEM	FMRPGKLSDY	FPKYPNPEA	-----ARA	ANNGALPPDL
				141-161 modeled in with		
				subunit 8: 34-54		
<i>RHOSH_cyt c1</i> :	SQLFN-GIGG	PEYIYSVLTG	FPEEPPKCAE	GHEPDGFYFN	RAFQNGSVPD	TCKDANGVKT
<i>BOVIN_cyt c1</i> :	SYIVRARHGG	EDYVFSLLTG	YCE-----	-----	----PPTGVS	LREGLYFNPY
<i>RHOSH_cyt c1</i> :	TAGSWIAMPP	PLMDDLVEYA	DGHDAVHAM	AEDVSAFLMW	AAEPKLMARK	QAGFTAVMFL
<i>BOVIN_cyt c1</i> :	FPGQAIGMAP	PIYNEVLEFD	DGTPATMSQV	AKDVCTFLRW	AAEPEHHRK	RMGLKMLLMM
<i>RHOSH_cyt c1</i> :	TVLSVLLYLT	NKRLWAGVKG	KKKTNV			
<i>BOVIN_cyt c1</i> :	GLLLPLVYAM	KRHKWSVLKS	RKLAYRP	PK		

Figure 7. Sequence alignment for cytochrome  $c_1$ . *RHOSH* is *R. sphaeroides bc<sub>1</sub>* complex.

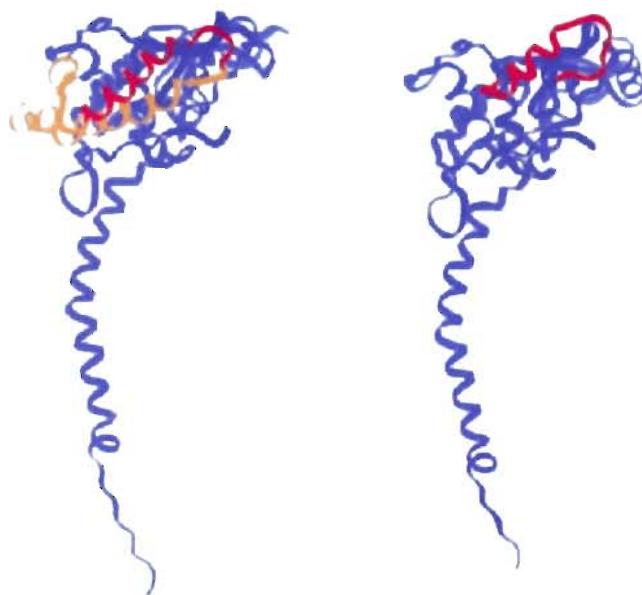


Figure 8. Cytochrome  $c_1$ . Bovine cytochrome  $c_1$  on left in blue. Subunit 8 on left in orange with the CSN in red and *R. sphaeroides* cytochrome  $c_1$  model on right with the template from the CSN in red.

```

RHOSH_ISP:                MSNAED HAGTRRDFLY YATAGAGAVA TGAAVWPLIN
BOVIN_ISP: SHTDIKVPDF SDYRRPEVLD STKSSKESSE ARKGFPSYLV TATTVGVA YA ARNVVSQFVS

RHOSH_ISP: QMNPSADVQA LASIFVDVSS VEPGVQLTVK FLGRPIFIRR RTEADIELGR SVQLGQLVDT
BOVIN_ISP: SMSASADVLA MSKIEIKLSD IPEGKNMAFK WRGRPLFVRH RTKKEIDQEA AVEVSQLRD-

          96-107 modeled in with secondary
          structure and molecular dynamics
RHOSH_ISP: NARNANIDAG AEATDQNR TL DEAGEWLVMW GVCTHLGCVP IGGVSGDFGG WFCPCGSHY
BOVIN_ISP: ----- -PQHDLERVK RP--E WVILI GVCTHLGCVP IANA-GDFGG YYCPCGSHY

RHOSH_ISP: DSAGRIRKGP APENLPIPLA KFI DETTIQL G
          | | | | | | | | | | | | | | | | | | | |
BOVIN_ISP: DASGRIRKGP APLNLEVPSY EFTSDDMVIV G

```

Figure 9. Iron Sulfur Protein (ISP) Sequence Alignment. RHOSH is *R. sphaeroides*.

Bov. ISP

Rs. ISP

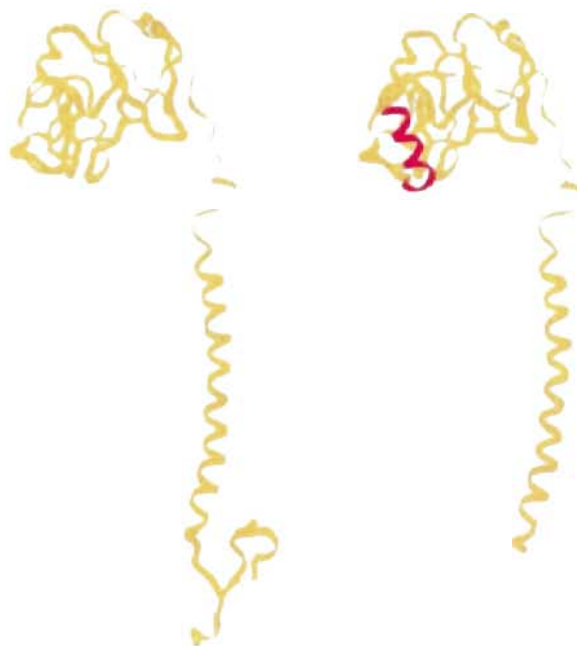


Figure 10. ISP 3D structure. On the left is bovine and on the right is *R. sphaeroides* with insertion in colored red.

#### IV. Subunit 4

The final subunit modeled is subunit 4. Subunit 4 has no significant homology with any of the other subunits in the bovine  $bc_1$  complex. Subunit 4 is similar to subunit 7 in the bovine because they both have the ability to be photo-affinity labeled by azido-quinone. Therefore, subunit 7 is used as a base template to model and build subunit 4 (Figure 11 and 12). A major problem encountered in this approach is that subunit 7 has a proline near the edge of the membrane causing the helix to kink inward (Figure 11). This proline is not in the *R. sphaeroides* subunit 4, so this region is modeled into a random coil to get the helix to change directions. A Blast search on subunit 4 sequence show there is another electron transfer protein, Aldehyde Ferredoxin Oxidoreductase (AFR), with some homology to subunit 4 (Figure 13 and 14) (20). The region with homology is significant because the structural features in this area, an alpha helix and a random coil, line up in pretty good agreement with the corresponding segment of the base model of subunit 4 built from subunit 7 of bovine (Figure 15). The last part of *R. sphaeroides* subunit 4 to be modeled is the N-terminal sequence. This modeling was accomplished by going back to the method of CSN to assign coordinates. After intense visual inspection of this area it was found that the core 1 has a CSN and this CSN, after further inspection, has some homology with subunit 4 sequence (Figure 16 and 17). Therefore the coordinates of core 1 residues 327-350 allow for the modeling of subunit 4 residues 1-24 (Figure 16 and 18). The complete theoretical model can now be assembled as shown in (Figure 19). The cytochrome *b* and cytochrome  $c_1$  hemes along with the iron sulfur cluster coordinates come directly from the bovine  $bc_1$  complex template hemes and iron sulfur cluster coordinates.



Figure 11. Bovine cytochrome *b* and subunit 7. In green cytochrome *b* and in red subunit 7.



Figure 12. *R. sphaeroides* cytochrome *b* and subunit 4. Cytochrome *b* in green and in red, subunit 4 from template. Purple is additional sequence.

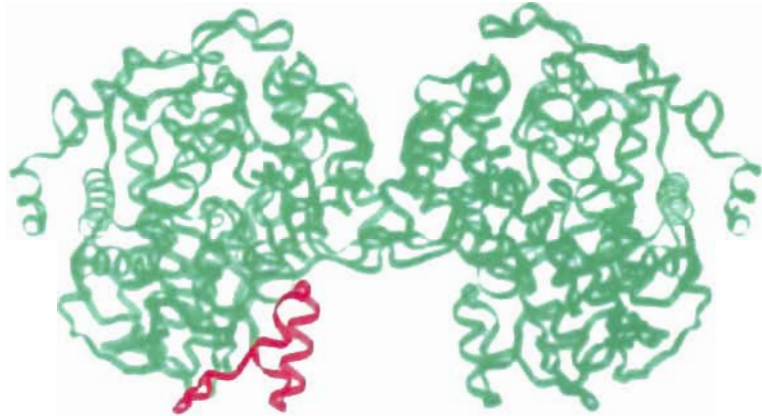


Figure 13. AFR. Shown in red color is the region with homology with subunit 4.

Rs. Subunit4:	44	LNDEELKIDPATWIWKRMP	SREEVAARRQRDFETV
AFR:	124	IKDEHIEIRDASHIWGKKV	SETEATIRKEVGSEKV

Figure 14: Sequence alignment for AFR and *R.sphaeroides* (Rs.) subunit 4.



Figure 15. AFR structural homology. *R. sphaeroides* cytochrome *b* green and subunit 4 in red. Shown in purple is the region that has homology with AFR.

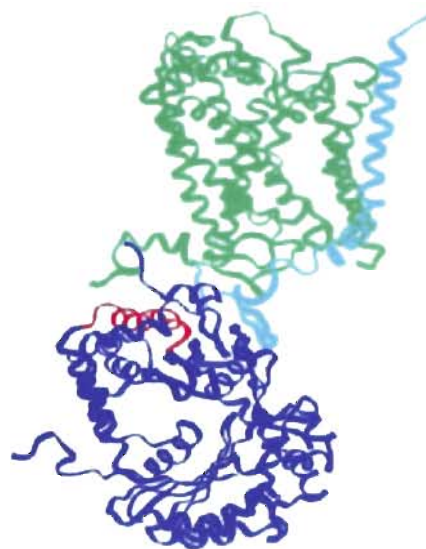


Figure 16. Bovine core 1 structural homology. Green is cytochrome *b* light blue is subunit 7 and dark blue is core 1 where CSN is colored in red.

Rs. subunit 4:	1	MFSFIDDIPSFEQIKARVR	DDLK	24
Bovine core1 :	327	DHMSIDDMMFVLQGQW	MRLCTSAT	350

Figure 17. CSN sequence alignment of bovine core 1 with *R. sphaeroides* (Rs.) subunit 4.



Figure 18. *R. sphaeroides* subunit 4 with CSN template. Cytochrome *b* in green and subunit 4 in red and highlighted in purple is the region built from the core 1 template.

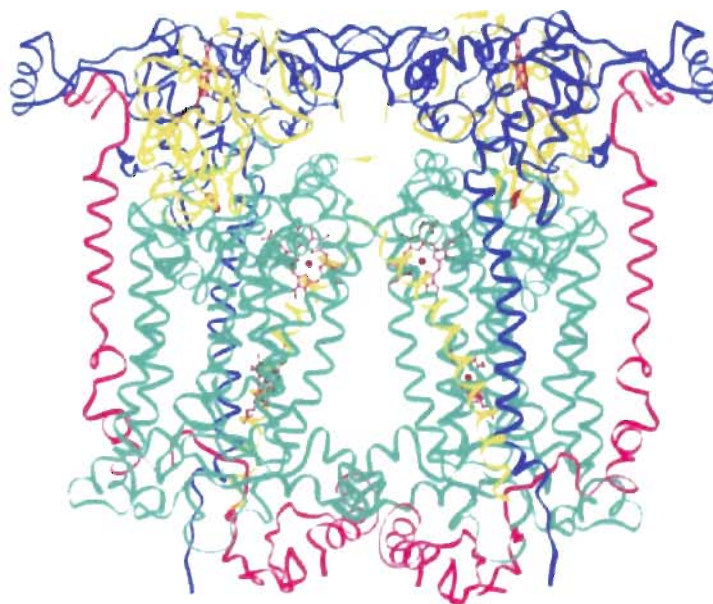


Figure 19. Theoretical model of *R. sphaeroides*  $bc_1$  complex. Cytochrome *b* in green, subunit 4 in red, cytochrome  $c_1$  in blue and iron sulfur protein in yellow.

## Conclusion

Subunits of *R. sphaeroides*  $bc_1$  complex are larger than their counter part in beef mitochondrial  $bc_1$  complex. By using a portion of the various extra subunits in beef  $bc_1$  complex, the extra insertions in *R. sphaeroides*  $bc_1$  complex were modeled in. The 3D model of the *R. sphaeroides*  $bc_1$  complex allows us to understand some structural possibilities that may be occurring. We see that the region in subunit 4 that has homology to the AFR complex exists on the outside of the complex in both the model and AFR crystal structure. The AFR complex is from a hyperthermophilic archaeon that grows optimally at 100 degrees Celsius (20). Therefore, the structural features of AFR play an important role in thermostability. The region where there is homology between AFR and *R. sphaeroides* subunit 4 in the model is located near the interface of the inner-membrane and outer-membrane region where cytochrome *b* begins to exit the membrane. It is possible that this region may play an important role in protecting this region of cytochrome *b* to allow for increased stability. It has been previously shown that residues 41-53 are essential for optimal interaction with the core complex to restore the  $bc_1$  complex activity (21,22).

Future directions for this modeling project would be first, to grow crystals to obtain a crystal structure of the *R. sphaeroides*  $bc_1$  complex. Second, to understand the interaction between cytochrome *b* and subunit 4 better, the electrostatic potential energy surface could be calculated and analyzed with a program called Delphi. Also further mutations in cytochrome *b* on the region of the subunit 4 and cytochrome *b* interface will aid in the understanding of possible functional roles of various residues.



## References

1. Browne, W.J., North, A.C.T., Philips, D.C., Brew, K., Vanaman, T.C., Hill, R.L. (1969) A Possible Three-dimensional Structure of Bovine-Lactalbumin based on that of Hen's Egg-White Lysozyme. *J. Mol. Biol.*, **42**, 65-86
2. Shotton, D.M., Watson, H.C. (1970) Three-dimensional Structure of Tosyl-elastase. *Nature*, **255**, 811-816
3. Greer, J. (1980) Model for haptoglobin heavy chain based upon structural homology. *Nat. Acad. Sci. U.S.A.*, **77**, 3393-3397
4. Greer, J. (1981) Comparative Model-building of the Mammalian Serine Proteases. *J. Mol. Biol.*, **153**, 1027-1042
5. Greer, J. (1985) Model Structure for the Inflammatory Protein C5a. *Science*, **228**, 1055-1060
6. Blundell, T.L., Sibanda, B.L., Sternberg, M.J.E., Thornton, J.M. (1987) Knowledge-based prediction of protein structures and the design of novel molecules. *Nature*, **326**, 347-352
7. Blundell, T.L., Carney, D., Gardner, S., Hayes, F., Howlin, B., Hubbard, T., Overington, J., Singh, D.A., Sibanda, B.L., Sutcliffe, M. (1988) Knowledge-based protein modelling and design. *Eur. J. Biochem.*, **172**, 513-520
8. Myers, R. A. (1995) *Molecular Biology and Biotechnology*, Wiley-VCH, NY.
9. Lemcke, T., Christensen, I.T., Jorgensen, F.S. (1999) Towards an Understanding of Drug Resistance in Malaria. *Bioorg. Med. Chem.*, **7**, 1003-1011
10. Huang, X., Zhang, H., Zen, K.C., Muthukrishnan, S., Kramer, K.J. (2000) Homology Modeling of the insect chitinase catalytic domain--oligosaccharide complex and the

- role of a putative active site tryptophan in catalysis. *Insect Biochem. Mol. Biol.*, **30**, 107-117
11. Yu, L., Yu, C. (1991) Essentiality of the Molecular Weight 15000 Protein (Subunit IV) in the Cytochrome *b-c1* Complex of *Rhodobacter sphaeroides*. *Biochemistry*, **30**, 4934-4939
  12. Shigeyuki, U., Yu, L. (1991) Subunit IV (Mr = 14,384) of the Cytochrome *b-c1* Complex from *Rhodobacter sphaeroides*. *J. Biol. Chem.*, **266**, 15644-15649.
  13. Yeong-Renn, C., Shigeyuki, U., Yu, C., Yu, L. (1994) Role of Subunit IV in the Cytochrome *b-c1* Complex from *Rhodobacter sphaeroides*. *Biochemistry*, **33**, 10207-10214
  14. Chen, Y., Shenoy, S.K., Yu, C., Yu, L. (1995) Identification of Amino Acid Residues Involved in Structural and Ubiquinone-binding Functions of Subunit IV of the Cytochrome *bc1* Complex from *Rhodobacter sphaeroides*. *J. Biol. Chem.*, **270**, 11496-11501
  15. Xia, D., Yu, C., Kim, H., Xia, J.Z., Kachurin, A.M., Zhang, L., Yu, L., Deisenhofer, J. (1997) Crystal Structure of the Cytochrome *bc1* Complex from Bovine Heart Mitochondria. *Science*, **277**, 60-66
  16. Iwata, S., Lee, J.W., Okada, K., Lee, J.K., Iwata, M., Rasmussen, B., Link, T.A., Ramaswamy, S., Jap, B.K. (1998) Complete Structure of the 11-Subunit Bovine Mitochondrial Cytochrome *bc1* Complex. *Science*, **281**, 64-71
  17. Zhang, Z., Huang, L., Shulmeister, V.M., Chi, Y.I., Kim, K.K., Hung, L.W., Crofts, A.R., Berry, E.A., Kim, S.H. (1998) Electron Transfer by Domain Movement in Cytochrome *bc1*. *Science*, **392**, 677-684

18. Kim, H., Xia, D., Yu, C., Xia, J., Kachurin, A.M., Zhang, L., Yu, L., Deisenhofer, J. (1998) Inhibitor Binding Changes Domain Mobility in the Iron-Sulfur Protein of the Mitochondrial *bcl* Complex from Bovine Heart. *Proc. Natl. Acad. Sci. USA*, **95**, 8026-8033
19. Altschul, S.F., Gish, W., Miller, W., Myers, E.W., Lipman, D.J. (1990) Basic Local Alignment Search Tool. *J. Mol. Biol.*, **215**, 403-410
20. Chan M.K., Mukund, S., Kletzin, A., Adams, M.W., Rees, D.C. (1995) Structure of a Hyperthermophilic Tungstopterin Enzyme, Aldehyde Ferredoxin Oxidoreductase. *Science*, **267**, 1463-1472
21. Yu, L., Tso, S.C., Shenoy S.K., Quinn, B.N., Xia, D. (1999) The Role of the Supernumerary Subunit of *Rhodobacter sphaeroides* Cytochrome *bcl* Complex. *J. Bioenerg. Biomembr.* **31**, 251-257
22. Tso, S., Shenoy, S.K., Quinn, B.N., Yu, L. (2000) Subunit IV of Cytochrome *bcl* Complex from *Rhodobacter sphaeroides*. *J. Biol. Chem.*, **275**, 15287-15294

## CHAPTER II

### MOLECULAR MECHANICS OF THE $bc_1$ COMPLEX

#### Introduction

##### I. Molecular Mechanics

Computational characterization of macromolecules plays an important role in understanding molecular properties of macromolecules. The process of computationally characterizing a macromolecule begins with using a well-parameterized function to model the molecular properties of the macromolecule. This function is usually called a force field. A force field consists of a potential energy expression functional form along with the complete set of parameters needed in order to determine the potential energy surface of the molecule (1). Force fields consider certain molecular attributes of a molecular system such as Coulombic potential, Van der Waals repulsion, bond length, valence angle, and torsion angle variables (2-9). In molecular mechanics the force field variables are optimized to locate the minimum potential energy of the molecular system. This can be of great benefit because it allows one to discover which conformation or which state of the molecular system is energetically favorable over the other (6).

The implementations of force fields have allowed an increase in understanding of molecular structures (10,11). The structure of androsterone was calculated by the force field (molecular mechanics) method (12). A review on the effective energy functions for protein structure prediction shows that molecular mechanics force fields, particularly

when augmented by implicit solvation models, provide physical effective energy functions that are beginning to play a role in the area of protein structure prediction, fold recognition and homology modeling (13).

## II. Cytochrome $bc_1$ complex

Cytochrome  $bc_1$  complex has a low potential cytochrome  $b_L$  heme, high potential cytochrome  $b_H$  heme, cytochrome  $c_1$  heme, and a 2Fe2S-cluster (Figure 20,21). In the proton motive Q cycle, ubiquinol is oxidized in two strictly coupled steps in which the first electron from ubiquinol is transferred to the 2Fe2S cluster of iron sulfur protein (ISP) then to cytochrome  $c_1$  (14). In the second step the second electron immediately reduces heme  $b_L$ , then heme  $b_H$  (14). ISP head domain mobility is known to be important in the transferring of the electron from ubiquinol to cytochrome  $c_1$  (15-19).

## III. Summary

Molecular mechanics will be used here to help determine which of the many backbone torsion angles are important for the mobility of the iron sulfur cluster with respect to its redox state. These computational results will be compared to preliminary static structural data obtained from x-ray diffraction experiments, and previously described mutational studies. Molecular mechanics will allow for the ability to pinpoint possible backbone torsion angles that are deviating significantly from the reduced state to the oxidized state of ISP.

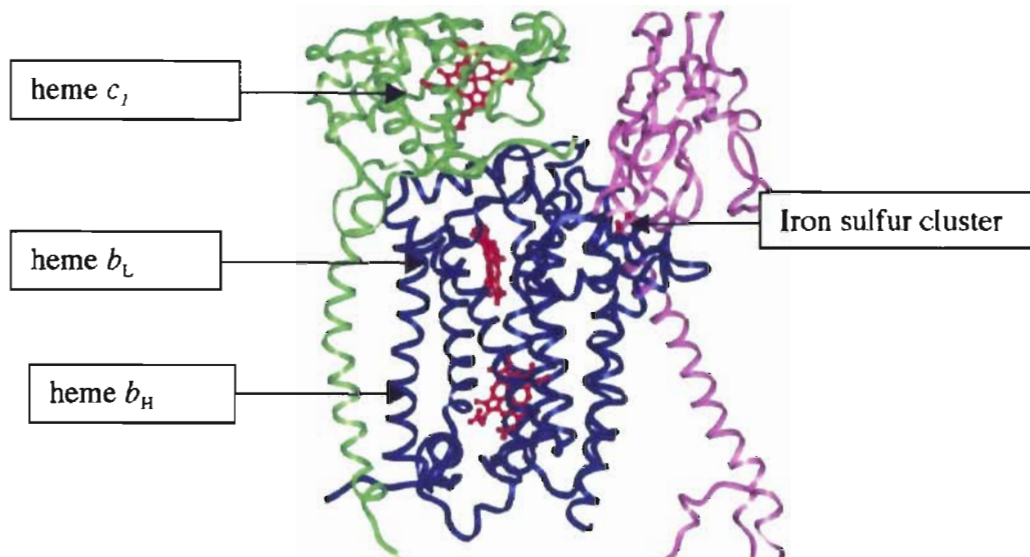


Figure 20. Cytochrome  $bc_1$  complex redox groups. Pink =ISP, blue = cytochrome  $b$  and green = cytochrome  $c_1$

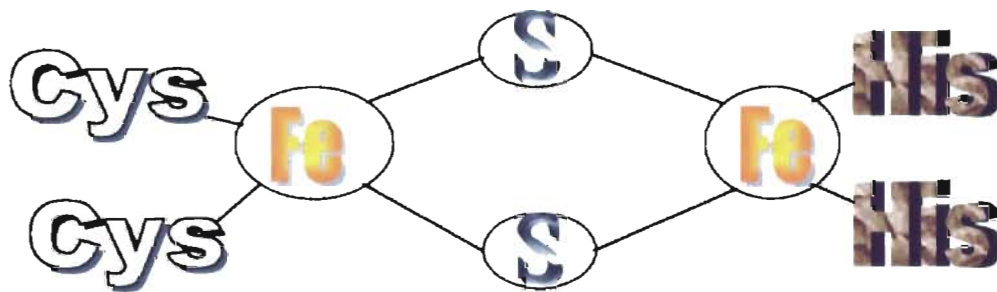


Figure 21. Iron Sulfur Cluster. Cys = cysteine, His = histidine, S = sulfur and Fe = Iron

## Methodology

InsightII molecular modeling software Discover3 is used to do all of the minimizations. The consistent valence force field (cvff) is used to do all the calculations. Minimization methods used are the steepest decent and conjugate gradient method. For cytochrome *b* and ISP the requirement for convergence is when the derivative reached 0.001. For cytochrome *c<sub>1</sub>* the requirement for convergence is when the derivative reached 0.500 instead of 0.001 because of the complexity of the potential energy surface for cytochrome *c<sub>1</sub>*. Calculations of all subunits are simulated in a vacuum. The iron atoms that are being oxidized and reduced are treated as a point charge in the subunits. The pdb coordinates that were used for the calculations come from the newly refined pdb coordinates (not yet released) from the original coordinates for the bovine *bc<sub>1</sub>* complex 1QCR.

For x-ray diffraction, data was collected at Brookhaven National Laboratory, where beam line X9B was used to collect data on the crystal with the inhibitor. Data for the reduced crystal form was also collected at Brookhaven National laboratory on beam line X9B. Diffraction reflections were processed with Denzo and Scale Pack. All other data processing was done with the Xtal View crystallographic program package.

## Results and Discussion

### I. Cytochrome *b* molecular mechanics

In checking the validity of the force field and the parameters for the atom types, three independent calculations were done on cytochrome *b*. The first calculation was a minimization of cytochrome *b* with heme  $b_L$  reduced and heme  $b_H$  oxidized which yielded a potential energy of 102 kcal/mole as seen in (Table I). Energy values for cytochrome *b* minimizations are normalized by dividing the value from the program by 25. The calculations are done on only one subunit at a time. Therefore, the significance is in the difference in magnitude of the energy values, for the independent subunits in different redox states. The root mean square (rms) obtained when the c-alpha trace of the minimized cytochrome *b* (reduced heme  $b_L$  and oxidized heme  $b_H$ ) structure was superimposed on the original structure (1QCR) c-alpha trace is 3.17 angstroms (Figure 22). In the second calculation the potential energy for cytochrome *b*, when heme  $b_H$  is reduced and heme  $b_L$  is oxidized, is 101 kcal/mol and in the third calculation, the potential energy when both hemes are oxidized is 82 kcal/mole (Table I). It is more favorable for heme  $b_H$  to be reduced than it is for heme  $b_L$  to be reduced. This is consistent with the proton motive Q cycle in that the electron goes from heme  $b_L$  to heme  $b_H$ . This data shows that the electron in the system is going from a higher potential energy state to a lower more favorable potential energy state. Realizing that the forcefield used in the computational analysis is empirical by nature these results are nevertheless in agreement with currently known knowledge of the electron transfer mechanism. Therefore, we



should be able to extrapolate and to detect critical residues that play an important role in conformational dynamics of the system. The rms when the  $b_H$  heme is reduced is 3.15 angstroms when compared to the original crystal structure. This difference in the backbone could be significant in terms of a possible slight conformational movement in cytochrome  $b$  helices that could correlate to the efficient binding of ubiquinone.

TABLE I  
CYTOCHROME  $b$  HEME ANALYSIS

Heme redox state	Potential Energy (kcal/mol)	rms
$b_L$ (reduced) – $b_H$ (oxidized)	102	3.16
$b_L$ (oxidized) – $b_H$ (reduced)	101	3.15
$b_L$ (oxidized) – $b_H$ (oxidized)	82	N/A

## II. Cytochrome $c_1$ molecular mechanics

Minimized cytochrome  $c_1$  has an oxidized potential energy of 117 kcal/mol and in the reduced form the potential energy is 569 kcal/mol. After superimposing the minimized oxidized and minimized reduced structures the rms was 0.28 (Figure 23). However, we can notice small deviations in some of the loop regions of the backbone when the minimized cytochrome  $c_1$  oxidized or reduced structures are superimposed on the original crystal structure (1QCR) for cytochrome  $c_1$  may be the result of not including all subunits in the calculation (Figure 24). The energy values obtained from this calculation are also in agreement with the underlying structure of the proton motive Q cycle.

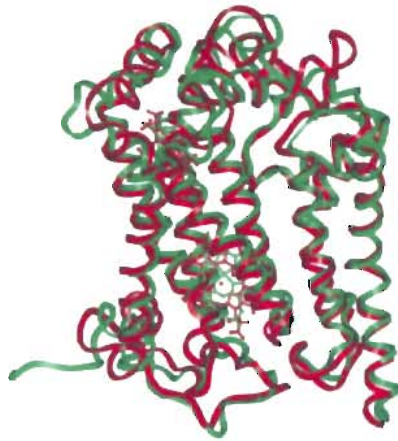


Figure 22. Cytochrome *b* redox state comparison. Original crystal structure (1QCR) in green and minimized heme *b<sub>L</sub>*(reduced) –heme *b<sub>H</sub>*(oxidized) in red.

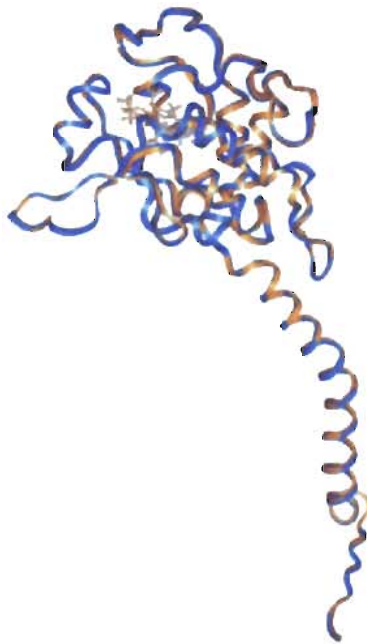


Figure 23. Cytochrome *c<sub>1</sub>* redox state comparison. Minimized cytochrome *c<sub>1</sub>* reduced in blue and minimized cytochrome *c<sub>1</sub>* oxidized in orange.

The oxidized cytochrome  $c_1$  heme is energetically more favorable than the reduced form. From the Q cycle mechanism, ISP transfers the electron to cytochrome  $c_1$ . Therefore, when the higher potential ISP head domain is in a position close to cytochrome  $c_1$  where it is more unfavorable for the 2Fe2S cluster to have the electron than it is for cytochrome  $c_1$  to have the electron, cytochrome  $c_1$  will gain the electron.

### III. ISP molecular mechanics

The molecular mechanics of ISP is very intriguing. From the first minimization, when the iron atom in the 2Fe2S cluster (Figure 21) that is coordinated to the histidines (his-Fe) is reduced and the iron atom coordinated to the cystines (cys-Fe) is reduced, we see that there is a potential energy of -1,308 kcal/mol (Table II). From a comparison of this minimized structure we see a significant difference in the head domain region as seen in (Figure 25) when the helix region is superimposed on the original crystal structure (1QCR) of ISP. Relative to cytochrome  $b$ , cytochrome  $c_1$  and ISP coordinates from the original crystal structure, the head domain position of minimized reduced ISP has moved closer to the cytochrome  $c_1$  (Figure 26). ISP displays significant conformational movement in relation to the minimization's done on cytochrome  $b$  and cytochrome  $c_1$ . This correlates with the x-ray diffraction analysis of ISP. The density for cytochrome  $b$  and cytochrome  $c_1$  are more defined and the ISP head domain in some crystal forms is not well defined which is an indication of mobility (20). In the next minimization where the cys-Fe reduced and his-Fe oxidized (ISP [2-3]) we see a potential energy of

TABLE II  
POTENTIAL ENERGY VALUEELS FOR ISP DIFFERENT REDOX STATES

Cys-Fe	His-Fe	Potential Energy (kcal/mol)
Oxidized	Reduced	-1,893
Oxidized	Oxidized	-2,609
Reduced	Reduced	-1,308
Reduced	Oxdized	-1,889

TABLE III  
ISP TORSION ANGLE ANALYSIS

Residue	Torsion Angle (degrees)*					
	Omega		Phi		Psi	
	Reduced	Oxidized	Reduced	Oxidized	Reduced	Oxidized
66 ALA	-14.65	-1.17	-67.01	-82.13	152.96	120.18
67 ASP	-6.55	-11.66	-70.53	-130.69	138.38	-154.22
68 VAL	-12.97	-1.62	65.08	51.24	125.55	86.26
89 PHE	-0.47	1.65	-88.48	-91.96	43.61	-39.58
93 GLY	12.92	-8.93	66.12	67.37	-124.44	88.23
111 ALA	1.74	-19.27	-80.32	-82.60	148.01	-147.47
116 GLN	-1.25	30.40	-70.62	-85.79	170.60	-123.20
141 HIS	-27.49	-15.76	-103.36	-79.20	136.34	45.97
161 HIS	4.69	1.64	82.10	62.59	115.58	-35.43
168 SER	-20.16	-1.82	-68.89	-83.04	164.67	-176.21

\*Oxidized form of ISP where cys-Fe is oxidized and his-Fe is oxidized. Reduced form of ISP is where cys-Fe is oxidized and his-Fe is reduced.

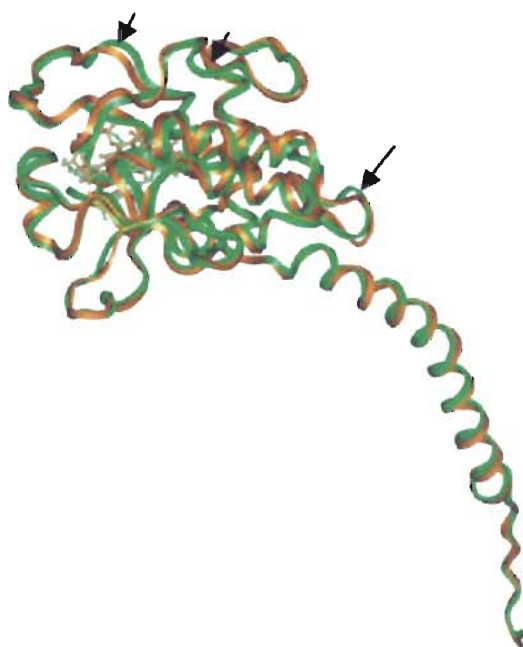


Figure 24. Cytochrome *c*, redox state comparison with original structure (1QCR). Minimized cytochrome *c*, oxidized in orange and original crystal structure of cytochrome *c*, in green the arrow point to areas of deviation

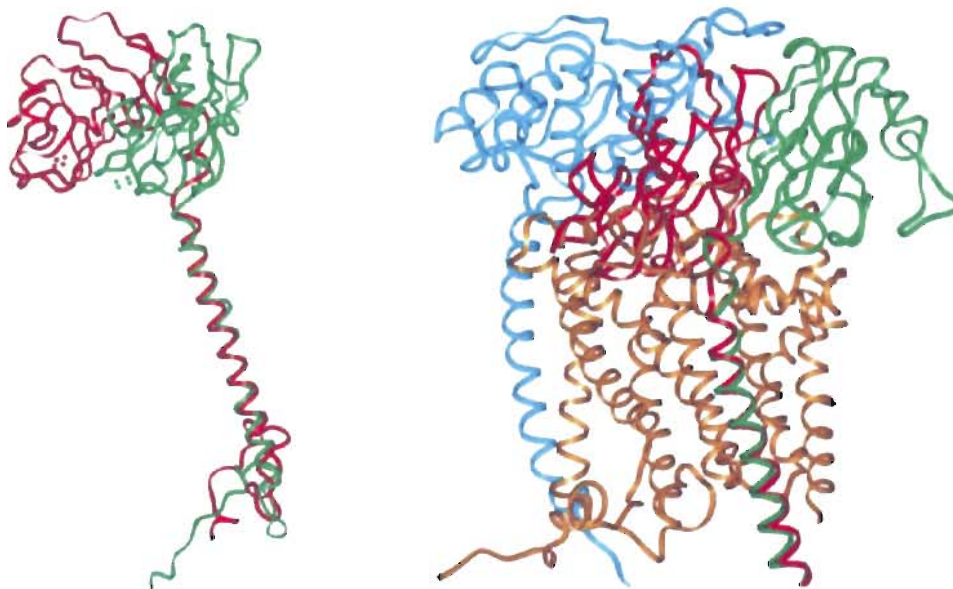


Figure 25. ISP with both irons reduced. Green is original crystal structure ISP and red is minimized ISP where cys-Fe and his-Fe are reduced.

Figure 26. Relative position of ISP with both iron atoms reduced. Orange is crystal original structure for cytochrome *b*, in light blue is crystal structure for cytochrome *c*<sub>1</sub>, green is crystal structure of ISP and red is ISP minimized where cys-Fe and his-Fe are both reduced.

-1,889 kcal/mol, and again we see significant deviation from the coordinates of the crystal structure ISP (Figure 27). Cys-Fe reduced and his-Fe oxidized form are farther from the original ISP head domain, and closer to cytochrome *c*<sub>1</sub> than the cys-Fe reduced and his-Fe reduced (ISP [2-2]) form (Figure 28,29). It is known that only the iron coordinated to the histidines in the 2Fe2S cluster is oxidized and reduced and the iron that is coordinated to the cysteine is always oxidized (21). So in order to determine how well this minimization compares to known information, calculations were done with both iron atoms in the 2Fe2S cluster oxidized (ISP [3-3]). In this calculation the potential energy was -2.609 kcal/mol (Table II). There is noticeable deviation in the head domain region when compared to the original crystal structure (Figure 30). In (Figure 31) we see that this position is close to the position for the ISP [2-3] form. When the iron coordinated with the cystine is oxidized and the iron coordinated to the histidine is reduced (ISP [3-2]) we see a potential energy of -1.894 kcal/mol and the head domain position is close to the original head position in the crystal structure (Figure 32).

This force field does a good job of reproducing known molecular data. The molecular mechanics calculations show that it is more favorable to have, the iron coordinated to the cysteine always oxidized. The computations were also able to reproduce the conformational movements of the ISP head domain. So we see from the computations that the reduced form of ISP head domain is energetically favorable closer to the cytochrome *b* and the head domain when oxidized prefers to be closer to the cytochrome *c*<sub>1</sub>. These are similar to results seen in preliminary x-ray diffraction data of crystals in different redox states. It seems reasonable that in the position above

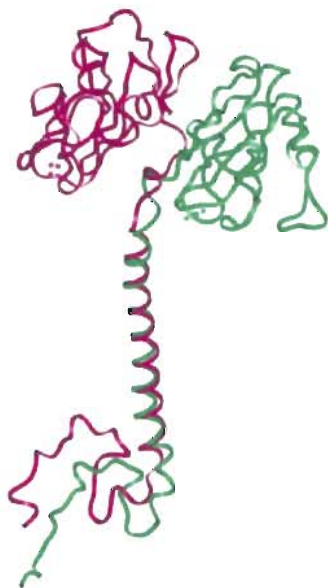


Figure 27. ISP [2-3] comparison. Where green is original crystal structure for ISP and in purple is the minimized ISP [2-3].

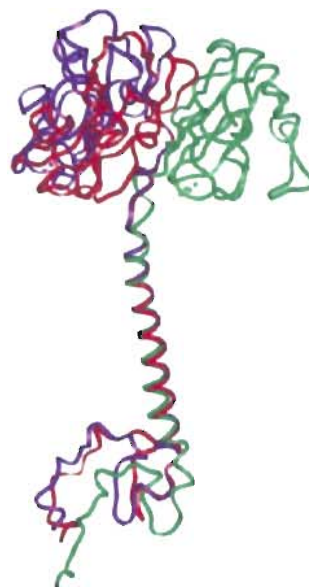


Figure 28. ISP [2-3] relative position. Where green is the original crystal structure for ISP and in purple is the minimized ISP [2-3] and in red is minimized ISP [2-2].

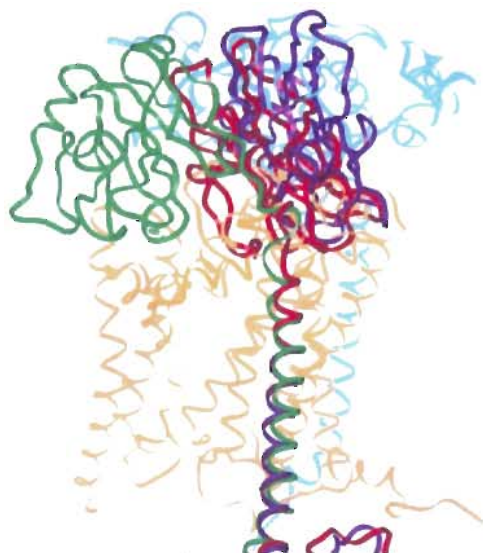


Figure 29. ISP [2-2] and [2-3] overall comparison. Where orange = original crystal structure of cytochrome *b*, light blue = original crystal structure for cytochrome *c*<sub>1</sub>, green = original crystal structure for ISP, purple = minimized ISP [2-3] and in red is minimized ISP [2-2].

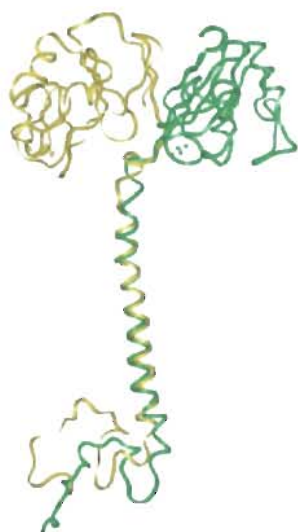


Figure 30. ISP [3-3] comparison, where green is the original ISP from crystal structure and yellow is minimized ISP [3-3].



Figure 31. ISP [3-3] and [2-3]. In purple is minimized ISP [2-3] where green is ISP from crystal structure and yellow is minimized ISP [3-3].

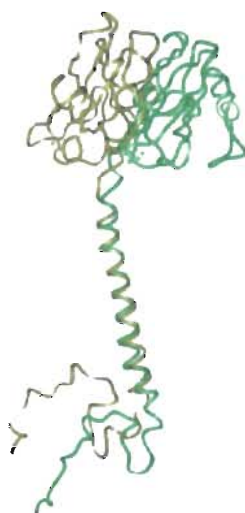


Figure 32. ISP [3-2] comparison. Where green is the original ISP from crystal structure and gold is minimized ISP [3-2].



cytochrome *b* ISP would prefer to have the electron. Because ISP needs to get the electron to give it to cytochrome *c*<sub>1</sub> and when the ISP head domain is close to cytochrome *c*<sub>1</sub> the head domain should not prefer to have the electron because it needs to give it to cytochrome *c*<sub>1</sub>.

#### IV. Torsion angle analysis

To further investigate where the movement is coming from an analysis of the backbone of the ISP is needed. The backbone torsion angles are very important in allowing the head domain movement. Therefore, a comparison of the backbone torsion angles in the oxidized and reduced minimized form is needed to determine where on the backbone there is strong deviation and movement occurring. The backbone of a protein has three torsion angles a phi, psi and omega as seen in (Figure 33).

ISP can be thought of as having 4 parts. A tail region; residues 1-28 that resides in the matrix, a body region; residues 29-63 that resides in the membrane, a neck region; residues 64-72 that resides in the inter-membrane space that is believed to be flexible and a head domain region; residues 73 - 197. From (Table III) we see that there is a large difference in the torsion psi angle for residue number 67. For the reduced ISP the torsion psi angle at residue 67 is 138.38 degrees and for the oxidized form the torsion psi angle is -154.22. This suggests, that this backbone psi torsion angle play an important role in the ISP head domain movement upon oxidation and reduction. If residue 67 was mutated to a proline this would completely restrict the psi torsion angle from being able to change. From studies on the bacteria *bc*<sub>1</sub> complex it has been previously found that upon mutating

residues 42-44 in the bacteria ISP, which corresponds to residues 66-68 in bovine ISP. with proline will inhibit photosynthetic growth (19). Further molecular mechanic simulations combined with individual mutations on each of these three residues can be done to determine how important residues 66 and 68 are in the head domain movement upon oxidation and reduction. However, from further investigation of the molecular mechanics computational data, the backbone at residue 67 has a very important role. As seen in (Table III) the torsion angles for residues 66 and 68 do not have a significant difference compared to the difference seen in residue 67. Residue 67 from visual inspections appears to be the better bond of the three for the linker region. Although any movement of the torsion angles plays a role in getting the head domain region in proper position for electron transfer, molecular mechanics calculations help determine where the most flexibility is.

When the structure of the  $bc_1$  complex was first solved it was noted that the ISP head domain appeared to be very mobile. This observation comes from the fact the electron density in the ISP head domain is not visible in some of the crystals of the  $bc_1$  complex. The results of the molecular mechanics calculations are in direct agreement with this conclusion. If the head were indeed very mobile and flexible it is possible that there is more than one flexible region. An example of this would be a chain, which is extremely flexible because it has a lot of links on it. Now consider if one were to restrict all the links on the chain and allow only one link to be flexible. It should be easy to see that by only having one link flexible results in a very rigid structure compared to the chain with many links in it. From doing the computation on the ISP we see that there is another psi

torsion angle at glycine 93 that has significant movement of -124.44 degrees for reduced form and 88.23 degrees for the oxidized form. This is of particular interest because of its location at the apex of a loop, which links the head of ISP to the neck region of ISP as seen in (Figure 34). By having this possible linker region would allow increased flexibility in the amount of positions that the head domain could take. If only one linker region exists then there would be a smaller number of rigid fixed positions and you would be more inclined to see some electron density of the iron sulfur cluster. However, if there are indeed two linker regions or more, the increased number of possible positions of the head domain positions would make the electron density peak of the ISP head domain difficult to detect.

#### V. Electron density comparison

Next is a basic comparison of torsion angles from the calculations and where density is observed in two different  $bc_1$  complex crystal forms. The first crystal form is with an inhibitor and the second crystal form is where ISP and cytochrome  $c_1$  are partially reduced. In (Figure 35) we see that there is a difference in the electron density peak for the inhibitor crystal form and the partially reduced crystal form at the 2Fe2S cluster. The inhibitor form has a greater peak as seen in the yellow color for the density. This suggests that the inhibitor help stabilize the 2Fe2S cluster whereas the peak for the reduced form is not as strong. This is an indicator that there may be some slight movement in the 2Fe2S position. In (Figure 36) ISP has significant density along the

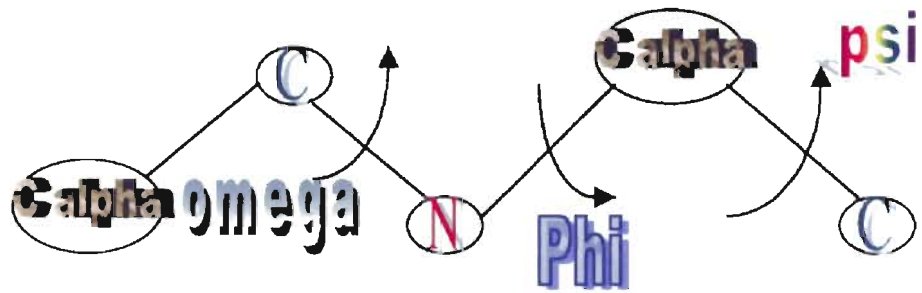


Figure 33. Protein back bone torsion angles.

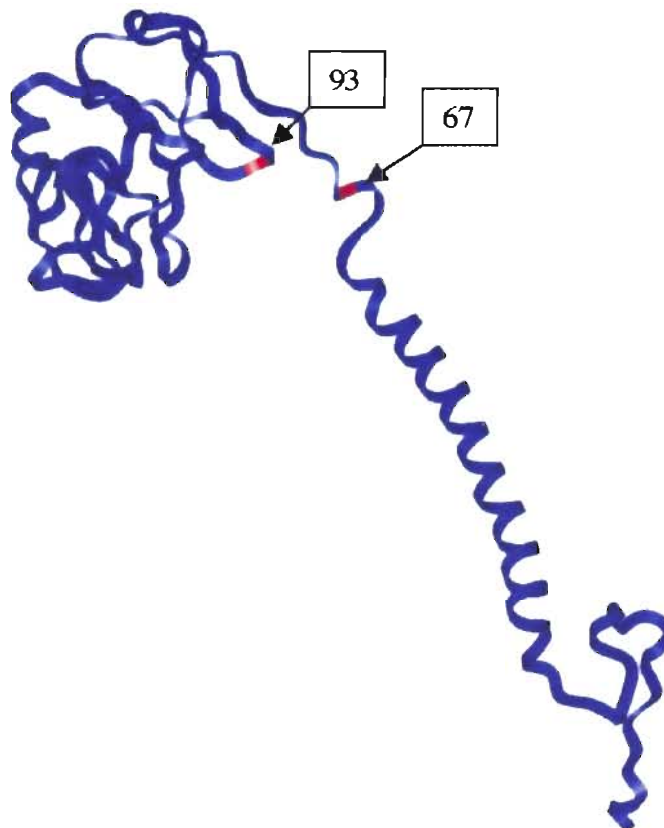


Figure 34. ISP linker regions. Where two of the linker regions are colored in red with residue number in square box.

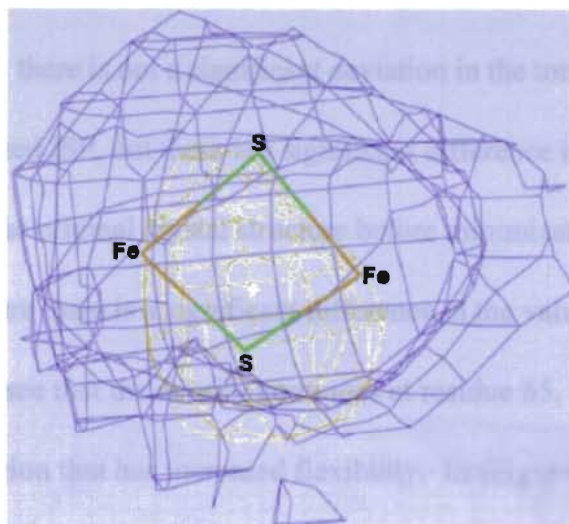


Figure 35. 2Fe<sub>2</sub>S cluster electron density map. Purple density is inhibitor form and in yellow is the reduced crystal form. Both maps are contoured at one sigma.

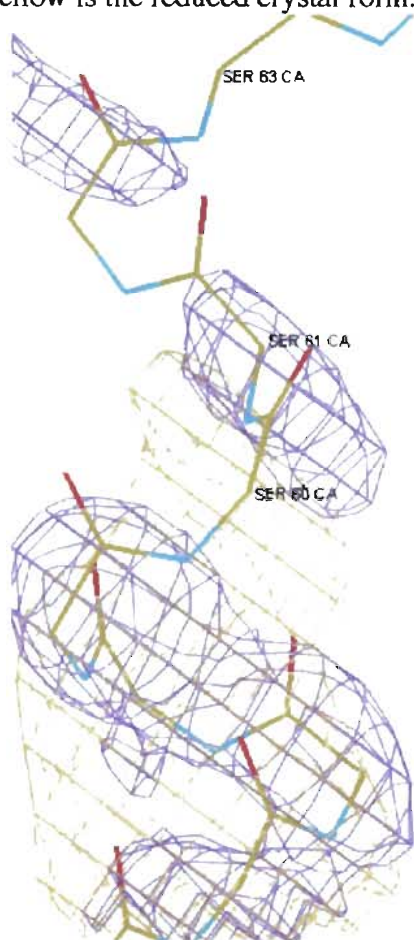


Figure 36. ISP electron density at serine 61 region.

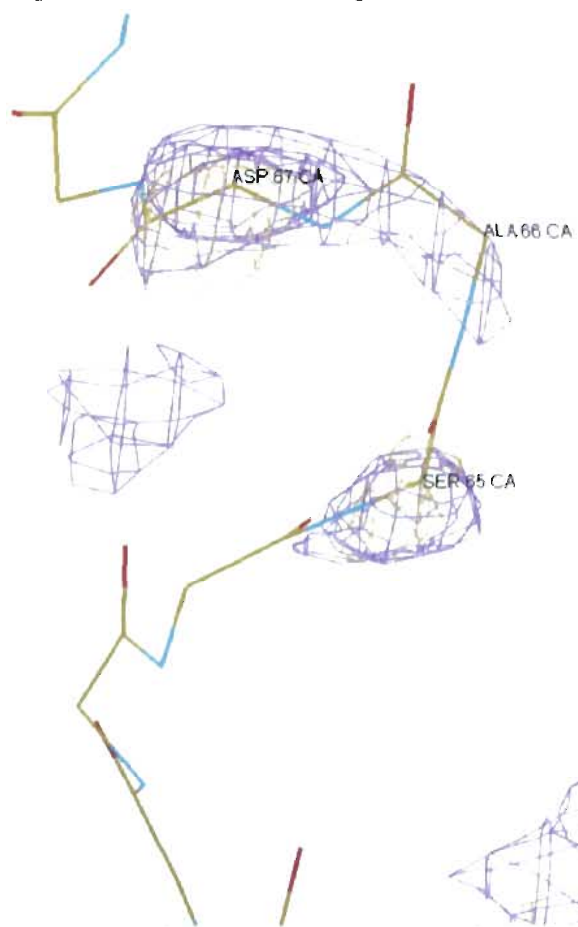


Figure 37. ISP electron density at serine 65 region.

transmembrane helix but starts to disappear around serine 61. This is an indication of where some of the torsion angles may have moved. From the calculation of the torsion angle at residue 61 there is not a significant deviation in the torsion angle values for the reduced and oxidized ISP, but there is a significant difference in the value of the psi torsion angle for the original crystal structure before minimization. Also at residue 62 in the original structure there is a significant difference in the value for the phi torsion angle. In (Figure 37) we see that the density continues at residue 65. From residues 61-65 there appears to be a region that has increased flexibility. In (Figure 38) the density continues to residue 68 for the inhibitor crystal form and then starts to vanish. However, for the reduced crystal form the density peak still shows up at residue 69, then it starts to vanish. From (Table III) the psi angle for residue 68 has some deviation. Molecular mechanics also show that the psi and phi angles at residue 70 have significant deviation between the original crystal form 1QCR and the minimized structures. In (Figure 39) residues 86-89 show higher density peaks for the inhibitor form and higher density peaks around residues 90-92 for the partially reduced form crystal. The rest of the ISP from this point on appears to be mobile except for the 2Fe2S-cluster region. From (Table III), the torsion angles, of residues 111-168 show a strong deviation that may play a role in the overall mobility of the head domain. This mobility appears to be a complex network of several distant torsion angles. Having more crystal forms with different inhibitors and different oxidation and reduction states for the prosthetic groups will allow for a more elaborate analysis of the torsion angles.



Figure 38. ISP neck region density. Blue density is the inhibitor crystal form and the green density is the reduced crystal form.

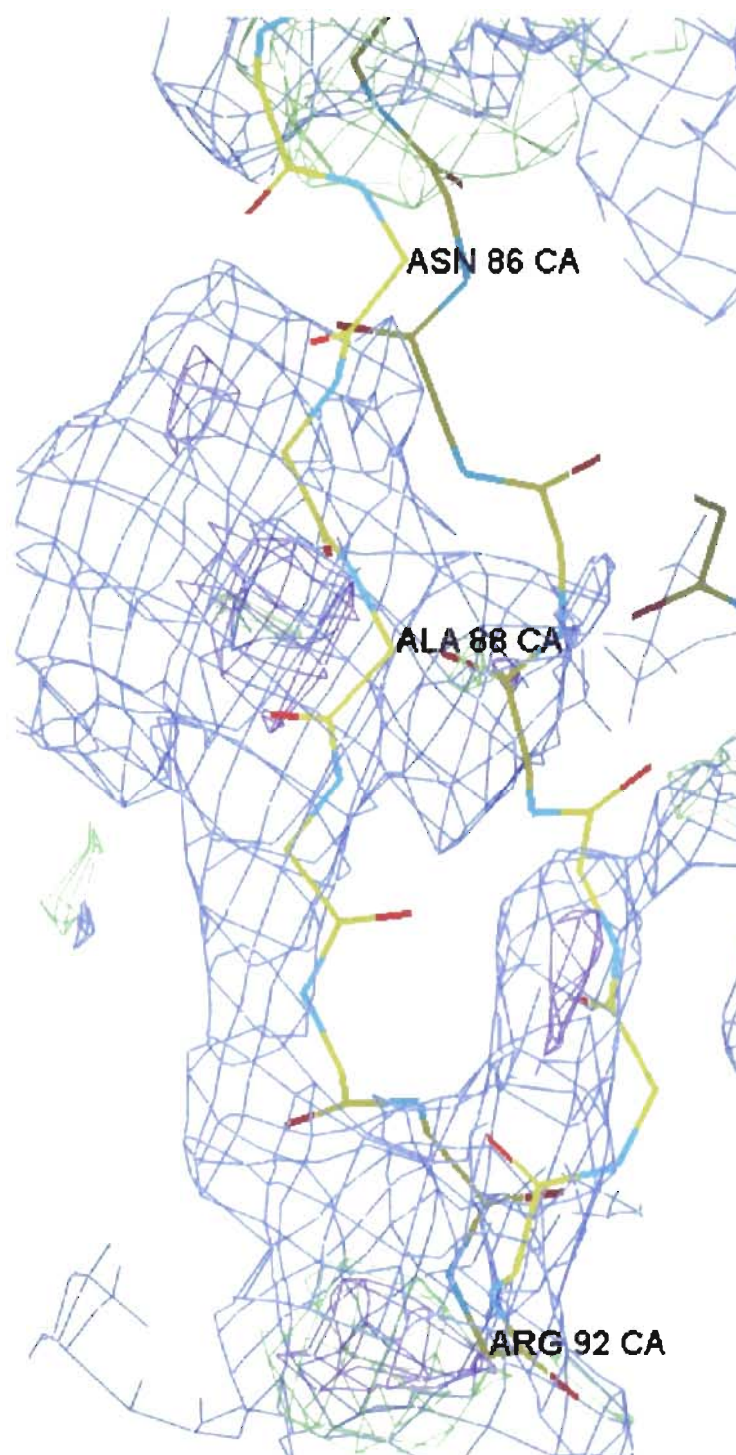


Figure 39. ISP electron density at residues 86-92. Blue density is contoured at one sigma for the inhibitor form the purple density is contoured at two sigma for the inhibitor form and the green density is contoured at one sigma for the reduced form.



## Conclusion

The force field used in these calculations is extremely powerful in modeling conformational aspects of this molecular system. The potential energy analysis is in agreement with the proton motive Q cycle. Torsion angle analysis comes very close to the preliminary x-ray diffraction data. In areas where there is weak density, the calculations help provide an indicator of the torsion angles that are deviating from their initial positions. Future directions would be to do an analysis on the individual iterations for the calculations to determine the sequence that the torsion angles are moving in. It would also be interesting to run electrostatic calculations to determine if the inhibitor binding might have any effect on any of these torsion angles.

In growing crystals of a protein it is very helpful to increase order in the crystal if flexible regions in the protein were restricted. Sometimes this can be accomplished by introducing prolines in the flexible regions to restrict torsion angle movement in the backbone of the protein. The next phase of this project should include site directed mutagenesis to insert the prolines in the areas where significant torsion angle differences are expected to determine 1.) if *in-vivo* these torsion angles play any significant role and 2.) if restricting these torsion angles with prolines will help facilitate the crystal growing process.

Modeling the basic functional properties of the  $bc_1$  complex will have a profound impact on the development of highly reasonable and accurate structure function predictions. Now that we have a model system, we can investigate the possible effect of

different theoretical inhibitors before labor intensive resources are deployed. We can use the affinity ligand-docking program in InsightII to computationally characterize the known active sites on the  $bc_1$  complex. This will help to provide reliable theoretical predictions of possible proton channeling paths. Combining computational results with site directed mutagenesis will help determine whether the predicted proton channeling path exist or not.

### References

1. Emer, O. (1976) Calculation of molecular properties using force fields. Applications in organic chemistry. *Structure and Bonding* **27**, 161-211
2. Cornell, W. D., Cieplak, P., Bayly, C. I., Gould, I. R., Merz, K. M. Jr., Ferguson, D. M. Spellmeyer, D. C., Fox, T., Caldwell. J. W., and Kollman, P. A. (1995) A second generation force field for the simulation of proteins, nucleic acids and organic molecules. *J. Am. Chem. Soc.* **117**, 5179-5197
3. Jorgensen, W. L.. & Tirado-Rives, J., (1988) The OPLS Potential Functions for Proteins. Energy Minimization for Crystals of Cyclic Peptides and Crambin. *J. Am. Chem. Soc.* **110**. 1657-1666
4. Brooks, B.R., Bruccoleri, R.E., Olafson, B.D., States, D.J., Swaminathan, S., Karplus, M. (1983) CHARMM: A program for macromolecular energy, minimization, and dynamics calculations. *J. Comp. Chem.* **4**, 187-217
5. MacKerell, A D ; Bashford, D; Bellott, M; Dunbrack, R L; Eva seck, J D; Field, M J; Fischer, S; Gao, J; Guo, H; Ha, S; JosephMcCarthy, D; Kuc nir, L; Kuczera, K;

- Lau, F T K; Mattos, C; Michnick, S; Ngo, T; Nguyen, D T; Pro hom, B; Reiher, W E; Roux, B; Schlenkrich, M; Smith, J C; Stote, R; Straub, J; W tanabe, M; WiorcikiewiczKuczera, J; Yin, D; Karplus, M (1998) All-atom empirical potential for molecular modeling and dynamics studies of proteins. *J. Phys. Chem. B* **102**, 3586-3617
6. Dauber-Osguthorpe, P.; Roberts, V. A.; Osguthorpe, D. J.; Wolff, J.; Genest, M.; Hagler, A. T. (1988) Structure and energetics of ligand binding to proteins: E. coli dihydrofolate reductase- trimethoprim, a drug-receptor system. *Proteins: Structure, Function and Genetics* **4**, 31-47
  7. Lii, J-H., Gallion, S., Bender, C., Wikstrom, H., Allinger, N. L., Flurchick, K. M., and Teeter, M. M. (1989) Molecular Mechanics (MM2) "Calculations on Peptides and on the Protein Crambin Using the Cyber 205" *J. Comp. Chem.* **10**, 503-513
  8. Lii, J-H., & Allinger, N. L. (1991) The MM3 Force Field for Amides, Polypeptides and Proteins. *J. Comp. Chem.* **12**, 186-199
  9. Halgren, T. A. (1996) Merck Molecular Force Field. II. MMFF94 van der Waals and Electrostatic Parameters for Intermolecular Interactions. *J. Comp. Chem.* **17**, 520-552
  10. Hwang, J. K., Warshel, A. (1987) Semiquantitative Calculations of Catalytic Free Energies in Genetically Modified Enzymes. *Biochemistry* **26**, 2669-2673
  11. Kitson, D.H., Avbelj, F., Moulton, J., Nguyen, D.T., Mertz, J.E., Hadzi, D., Hagler, A.T. (1993) On Achieving Better than 1-A Accuracy in a simulation of a large

- protein: *Streptomyces griseus* protease A. *Proc. Natl. Acad. Sci. USA*, **90**, 8920-8924
12. Allinger, N.L., Tribble, M.T., Yuh, Y. (1975) Androsterone. The Structure by Force-Field Calculations. *Steroids* **26**, 398-406
13. Lazaridis, T., Karplus, M. (2000) Effective Energy Functions for Protein Structure Prediction. *Curr. Opin. Struct. Biol.* **10**, 139-145
14. Brant, U. (1994) *Critical Reviews in Biochemistry and Molecular Biology*, **29**, 165-197
15. Xiao, K., Yu, L., Yu, CA. (2000) Confirmation of the Involvement of Protein Domain Movement During the Catalytic Cycle of the Cytochrome *bc1* Complex by the Formation of an Intersubunit Disulfide Bond Between Cytochrome *b* and the Iron-Sulfur Protein *J. Biol. Chem.*, paper in press
16. Yu, CA., Tian, H., Zhang, L., Deng, KP., Shenoy, S.K., Yu, L., Xia, D., Kim, H., Deisenhofer, J. (1999) Structural Basis of Multifunctional Bovine Mitochondrial Cytochrome *bc1* Complex. *J. Bioenerg. Biomembr.* **3**, 191-199
17. Izrailev, S., Crofts, A.R., Berry, E.A., Schulten, K. (1999) Steered molecular dynamics simulation of the Rieske subunit motion in the cytochrome *bc(1)* complex. *Biophys. J.* **77**, 1753-1768
18. Tian, H., White, S., Yu, L., Yu, CA. (1999) Evidence for the head domain movement of the rieske iron-sulfur protein in electron transfer reaction of the cytochrome *bc1* complex. *J. Biol. Chem.* **274**, 7146-7152

19. Tian, H., Yu, L., Mather, M.W., Yu, CA. (1998) Flexibility of the neck region of the rieske iron-sulfur protein is functionally important in the cytochrome *bc1* complex. *J. Biol. Chem.* **273**, 27953-27959
20. Xia, Di., Yu, CA., Kim, H., Xia, J.Z., Kachurin, A.M., Zhang, L., Yu, L., Deisenhofer, J. (1997) Crystal Structure of the Cytochrome *bc1* Complex From Bovine Heart Mitochondria. *Science* **277**, 60-66
21. Link, T.A., Iwata, S. (1996) Functional implications of the structure of the 'Rieske' iron-sulfur protein of bovine heart mitochondrial cytochrome *bc1* complex. *Biochim. Biophys. Acta* . **1275**, 54-60

VITA

Byron N. Quinn

Candidate for the Degree of

Master of Science

Thesis: HOMOLOGY MODELING AND MOLECULAR MECHANICS OF THE  $bc_1$  COMPLEX

Major Field: Biochemistry and Molecular Biology

Biographical:

Education: Graduated from Jennings Senior High, St. Louis, Missouri in June 1992; received Bachelor of Science degree in Chemistry from Langston University, Langston, Oklahoma in May 1997. Completed the requirements for the Master of Science degree with a major in Biochemistry and Molecular Biology at Oklahoma State University in December, 2000.

Experience: Graduate research assistant; Oklahoma State University, Department of Biochemistry and Molecular Biology, 1997 to present.

Professional Memberships: N.A.